



NUMERICAL AND EXPERIMENTAL INVESTIGATION OF NON-LUBRICATED AIR SCROLL EXPANDER DERIVED FROM A REFRIGERANT SCROLL COMPRESSOR

Aparna Kottapalli^a, Ramakrishna Konijeti^{b*}

^aResearch Scholar, Department of Mechanical Engineering, Koneru Lakshmaiah Education Foundation, Guntur-522502, Andhra Pradesh, India

^bProfessor, Department of Mechanical Engineering, Koneru Lakshmaiah Education Foundation, Guntur-522502, Andhra Pradesh, India

Corresponding author: ^{b*}konijeti95@gmail.com.

ABSTRACT

Scroll technology is widely used in refrigerators as compressors. This research paper presents the performance of a scroll-type expander derived from a scroll compressor. The research is carried out at low pressures. The effect of mechanical load on performance has been evaluated using compressed air as a working fluid. Two stages of the evaluation process are carried out in this research. In the first stage, the scroll expander model is numerically simulated using the CFD approach to predict the factors influencing the scroll expander performance. In the later stage, an experiment is carried out on a scroll-type expander prototype developed from a scroll compressor. To find the torque fluctuations with load, a rope and brake dynamometer system is adopted. The developed prototype can work as a scroll expander in the low-pressure range which is chosen between 2.75 bars to 4.13 bars. From the simulation analysis, the mass flow rate, speed, and pressure are predicted factors that affect the performance of a scroll-type expander. From the experimental results with varying mechanical loads, the scroll efficiency and volumetric efficiency change with pressure ratios are evaluated. CFD simulation has been repeated with input conditions to validate the developed CFD model. A mesh independency test has been done to confirm the accuracy of the CFD numerical simulation findings.

Keywords: Scroll expander, Load analysis, Scroll Efficiency, CFD Simulation, Performance.

1. INTRODUCTION

Low-grade energy sources have become more important in recent energy trends. Scroll technology has grown in relevance due to its versatility. In the low-grade energy utilization category, scroll technology is used in the refrigeration, air conditioning, and heat pump industries. Scroll-type expanders are widely applicable as secondary devices in various thermodynamic cycles. Scroll systems, use the energy available from sources like exhaust gases of internal combustion engines (YijiLu, 2017), biomass (Moro & Pinamonti, 2008), waste heat from industry (ClaudioCampana, 2019), (DOE:US, 2017), thermal energy from solar panels (Dieckmann, 2017), and heat energy from geothermal sources (Lu, 2015). From the review, it can be determined that scroll-type expanders are well-suited for the generation of low-grade power.

WHR (Waste Heat Recovery) using ORC (Organic Rankine Cycle) is one of its principal applications of scroll-type expanders. To improve the scroll-type expander efficiency as a generator, extensive research has been conducted on scroll profiles (Simon Emhardt, 2018). With pressurized air as the working fluid, they perform well as battery chargers. Scroll-type expanders are useful as power production equipment in various industries as they can work with a variety of working fluids ranging from refrigerants to steam (Narasimhan, 2019) and with compressed air (Qiu et al., 2018). These scroll-type expanders have extremely low vibration, noise, and friction, giving them even

additional advantages when it comes to replacing equipment in automobiles for smooth, frictionless operation (Fatigati et al., 2022). They can also work in both dry and wet conditions, which is useful in heat-generating applications.

The operation of the scroll machine is very simple and makes its simplicity a major factor in many industries. The other factors like compactness and durability are the added advantages of the scroll machine. These factors make it a viable choice as an expander in various industries including small-scale ORC systems (Fatigati, 2020). The scroll expander was divided into three major categories like hermetic scroll-type expanders, semi-hermetic scroll-type expanders, and open scroll-type expander drive expanders were studied in the literature study done by Fatigati (Fatigati, 2020) in the year 2020. A review by Fatigati (Fatigati, 2020), studied a small-scale ORC-based test bench. The working fluid considered in the study is R134a for debuting a hermetic scroll expander. The scroll-type expander used in the study is derived from a compressor and used three poles asynchronous engine for integrating the hermetic scroll-type expander developed.

1.1 Literature Review

Scroll expander application in the automobile industry has been tested (Fatigati et al., 2022). In this research, the scroll expander's feasibility as a dual intake port is analyzed. Similarly, research on a large number of micro- to small-scale organic Rankine cycle (ORC) applications are

* Corresponding Author Email Address: : konijeti95@gmail.com

conducted by Ramin Moradi (RaminMoradi et al., 2021). In this analysis, many researchers (RaminMoradi et al., 2021) used scroll compressors and transformed them into expanders. In the past ten years (1-8), several studies have tested and modeled scroll expanders. For scroll-type expanders, there is no other type of built-up volume. Therefore, depending on the scroll-type expander in question, the ideal pressure ratio changes. The power output is dependent on the scroll volume being taken into account. This analysis mainly focused on organic Rankine cycle systems to evaluate their performance. A review on the advantages of scroll expanders for low-pressure applications has been given by researchers like Miftah (Hijriawan et al., 2022). In their analysis, it has been concluded that the low flow rate and rotational speed, with a high-pressure ratio, dominate systems that are with a low capacity of less than 5kW.

Due to the release of different kinds of hazardous gases like CO, NO2, etc. into the atmospheric air (Tomasz et al., 2022) during the generation of thermal and electrical energy, there will be degradation and also detrimental impacts on human health. There will also be an effect on energy production from waste heat sources if suitable equipment is not selected for the generation of electricity. There will be a large increase in power production if accurate energy price forecasting is done before choosing the equipment for the chosen range of pressure and temperature available at WHR. This can result in savings in electricity between 23% and 35%, as the data demonstrate (Tomasz et al., 2022). In the recent literature review (Wei et al., 2022), the scroll-type expander's application is refined only to power generation, design, leakage loss and works in a higher pressure range.

As it can forecast far in advance of experimentation, utilizing sophisticated simulation software such as CFD has recently gained popularity. Researchers may use computational fluid dynamics (CFD) to Design, model and simulate experimental conditions using CFD. Researchers like Elyazid Flilihi (Flilihia et al., 2021) present the full heat transfer process for a variety of realistic geometric layouts and settings. Recent research (Flilihia et al., 2021) has focused on the computational analysis of natural convection heat transfer for windows using porous screening material. In their research, (Flilihia et al., 2021) presented a review on different aspects of CFD and also a detailed review of a flat plate's laminar forced convection flow. Depending on the boundary conditions, input, and output in a CFD analysis, a variety of mesh independence tests are available. Nusselt number has been used by researchers like Farhan Lafta Rashid. *et.al.* (LaftaSarmad et al., 2022). To test the mesh independence. In their analysis, the Nusselt number is used to numerically check the thermal performance in the heat exchanger, and the Zukauskas correlation is used to compare the mesh independency with the Nusselt number as a varying parameter.

To extend scroll-type expanders to other industries like automobiles and for low-pressure range applications, their performance has to be evaluated. Many researchers now have done the work on assessing the performance of a scroll compressor turned to expander only at high pressure. However, the pressure of the gases released in waste heat regenerators is low the present work is aimed to investigate the performance of scroll expanders at low pressure. In this regard, to find its performance under mechanical load-varying conditions, an experimental test has to be conducted. A CFD model is developed to predict the performance of a scroll-type expander before building a prototype. The availability of scroll-type expanders is less, in this current research work, a scroll compressor ZR28KM-PFZ-582 is used to develop a scroll-type expander prototype. This prototype is experimentally tested for performance evaluation.

2 NUMERICAL MODELING

2.1 CAD Modeling of a Scroll Geometry

In geometric modeling, the scroll pair is made using a variety of curve profiles, including involute, Archimedes spirals, and segmental arcs.

Many researchers employ a scroll pair and Lee. *et.al* (Lee & Wu, 1996) conducted a study on several theorems relating to planar orbiting processes (Fatigatib, 2020).

The functioning of a scroll involves the movement of a rotating scroll over a fixed scroll, which is a difficult geometric configuration. The scroll wraps in scroll-type expanders are involute circles of a consistent thickness. Between the stator and rotor, there is an inlet port. To ensure an even distribution of pressure, this scroll stator and rotor combination is positioned eccentrically. Chambers are created by the scroll pair. Zhiwei Ma's baseline approach is used to compute the volume in each chamber in terms of crank angle (Zhiwei, et al., 2016). According to (Zhiwei et al., 2016), the moving scroll is engaged with the fixed scroll at the baseline, generating crescent-shaped chambers. These chambers are set up so that they are at conjugate positions at an angle of 180 degrees. The baseline for creating the scroll profile is taken into account when calculating the volume of each chamber in this model. For geometric details and to transform it into a scroll expander prototype for experimentation, a scroll-type compressor ZR28KM-PFZ-582 is employed. The figure1 shows a schematic of a scroll-type expander.

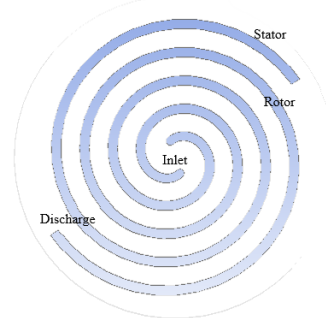


Fig. 1 Schematic of Scroll-type Expander

Expansion takes place in chambers of the scroll-type expander. Suction, expansion, and discharge are all performed while the scroll expander is in operation. Creo 6.0 is used to create the constant wall thickness scroll shape, while Ansys 15 is used to conduct the analysis. After being imported and meshed in the Ansys environment, the schematic scroll type expander with constant wall thickness is shown in Figure 2.

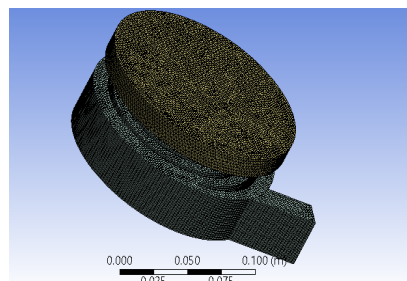


Fig. 2 3D model for Scroll Expander.

Table 1 Geometric parameters of scroll type expander

Terminology	Parameter	Value
The radius of the base circle	$r_b(m)$	5.02 $\pm 0.5 \times 10^{(-3)}$
Height of scroll	$H(m)$	$35 \pm 0.5 \times 10^{(-3)}$
Thickness of Scroll	$t_s(m)$	$4.2 \pm 0.5 \times 10^{(-3)}$
Initial involute angle	$\varphi (^{\circ})$	32
Radial Clearance	δ_r	6×10^{-5}
Axial Clearance	δ_f	6×10^{-5}

2.2 Boundary conditions

In the research project, numerical modeling utilizing CFD analysis is done in Ansys Fluent. This analysis's major emphasis is on the mass flow rate at the output, forces, and moments of the scroll expander prototype, along with a performance evaluation. The highest and lowest torques that are produced during the application of a mechanical load in an experiment are noted. The inputs for a scroll expander are mass flow rate at a predetermined speed, pressure, and inlet air temperature. As a result, the analysis's chosen boundary conditions are mass flow rate, pressure, and temperature. The stator, rotor, outlet, and working chambers of the bottom plate make up the domain under investigation, which is shown in Figure 3. The stator, rotor, and case are considered walls in the analysis.

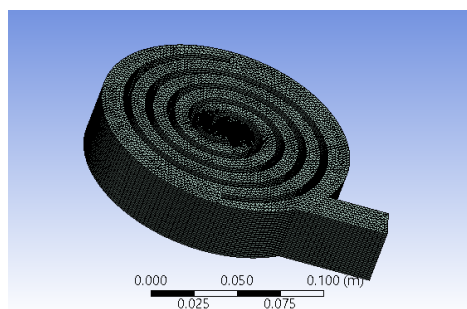


Fig. 3 Meshing of the bottom plate.

2.3 Flow Modeling

A dynamic mesh method is employed to simulate the scroll type expander. The eccentric movement of the orbiting scroll with respect to the fixed scroll was produced using the macros that are available in dynamic mesh technology offered by Ansys Fluent (ANSYS, 2015). The CG Motion macro in fluent's UDF controls the mesh motion has been adopted and the orbiting scroll in the scroll-type expander is assumed that the rotor rotates around the gravity center and is assumed to be at a steady pace. In scroll geometry, local remeshing and smoothing techniques are utilized to maintain mesh quality, while skewness and grid refinement are used for axial and radial clearance while modifying the enclosed working chamber volumes.

Transient conditions are taken into consideration in the UDF code (ANSYS, 2015). All of the governing equations that are mentioned in the Ansys guide (ANSYS, 2015) for continuity, solving momentum, and energy conservation are taken into account. In Ansys v15, the FVM approach is used for simulation. The Reynolds Averaged Navier – Stokes turbulence with the first-order upwind schemes is used for fluid flow study. To improve and identify swirl flows, renormalization (RNG) and k-epsilon model equations are applied. No-slip boundary conditions are applied for the walls of the domain under consideration. The PISO solver and the PRESTO pressure segregation method using the first-order implicit unsteady formulation are used to calculate pressure-velocity coupled equations. Simulation has been started for in-depth analysis for 0.015 seconds until convergence is reached. The time step considered is adaptive and is ranging from $1e^{-5}$ to $5e^{-5}$. The following are the governing equations for calculating mass flow rate in fluent.

$$\frac{\partial p}{\partial t} + \nabla(\rho v) = S_m \quad (1)$$

Where S_m denotes the source mass, ρ , and v are the density and volume. The mass flow rate at a pressure of 2.75, 3.44, and 4.13 bar has been evaluated at different loads ranging from 1kg to 2.5kg.

$$F_n = \frac{\vec{a}}{a} F_p + \frac{\vec{a}}{a} F_v \quad (2)$$

The built-in volume of the scroll expander generates the required work for driving the shaft attached to the orbiting scroll. F_p and F_v are the pressure and viscous forces acting on the walls of the rotor in tangential and vertical directions. Whereas 'a' is the coefficient of forces constant. The following relations are used to solve the force equations

and moment equations from the force equations given in equation 2. R_{AB} is the orbiting radius and is given as 5×10^{-3} meters.

$$M_A = \vec{r}_{AB} \times \vec{F}_p + \vec{r}_{AB} \times \vec{F}_v \quad (3)$$

The total moment, M_A is equal to the sum of the pressure and viscous moments. The perpendicular direction of the line of action of the force. r_{AB} is the moment vector. Table 3 of the manufacturing catalog lists the technical specifications of ZR28KM-PFZ-582.

2.4 Mesh independency test

In this study, CFD numerical verification is done by mesh independency test. The study involves testing the reproducibility and to make the solution lack discretization mistakes associated with mesh (Panigrahi et al., 2020). Making mesh or grid independence confirms the resulting solution's invariance with the number of elements as the mesh is improved. As per the mesh independency test, the computed solution should arrive at a non-deviating singular solution as the mesh is modified from coarse or large elements to fine or smaller elements. Mesh independency study has been conducted for mass flow rate, pressure, temperature, net forces, and moment for the developed CFD model.

Three distinct meshes were tested for the grid convergence study. One with a medium, fine, and a coarse grid was generated at the same pressure and boundary conditions. This test is conducted for all simulation conditions under study. The output values of mass flow rate, temperature, forces, moment, and pressure are presented in a graphical representation taken at 2.75 bar pressure and 307 K temperature. The force and moment obtained presented are also taken at 2.75 bar pressure, 307 K, speed of 1147 rpm, and mass flow rate of 0.028 kg/s. The graphical representation for mass flow rate at outlet, temperature, pressure, forces, and moment has been given in Figures 4-8. Table 2(a), 2(b) gives CFD validation for Mesh independency test.

Table 2(a) Mesh independency test

Element type	Number of elements	Mass output	Pressure output(pascal)	Temperature output(k)
Coarse	139335	1.02E-03	89900	306
Medium	197004	1.03E-03	1E+05	307
Fine	398225	1.03E-03	1E+05	307

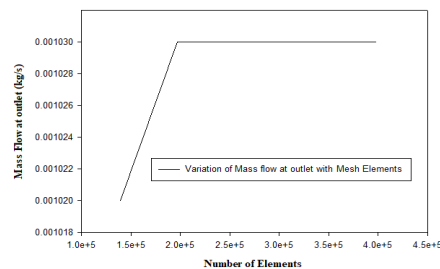


Fig. 4 Mesh independency test for outlet Mass flow rate.

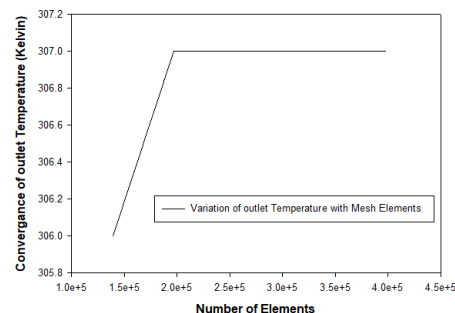


Fig. 5 Mesh Independency test for outlet temperature.

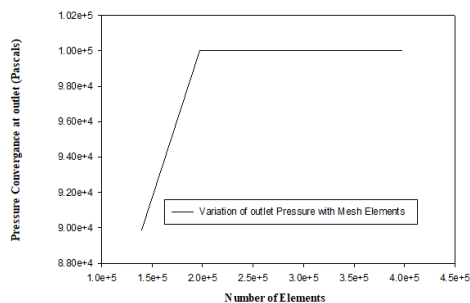


Fig. 6 Mesh independency test for outlet Pressure.

Table 2(b) Mesh independency test

Element type	Number of elements	Forces Output(N)	Moment output(N-M)
Coarse	139335	1.08E-03	1.23
Medium	197004	1.03E-03	1.25
Fine	398225	1.03E-03	1.25

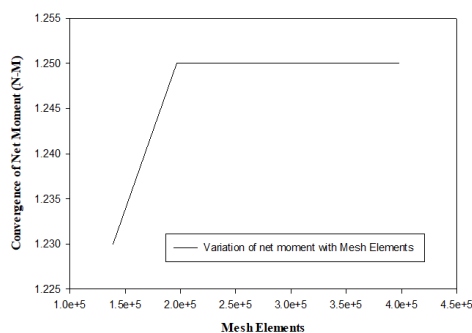


Fig. 7 Mesh independency test for the net moment

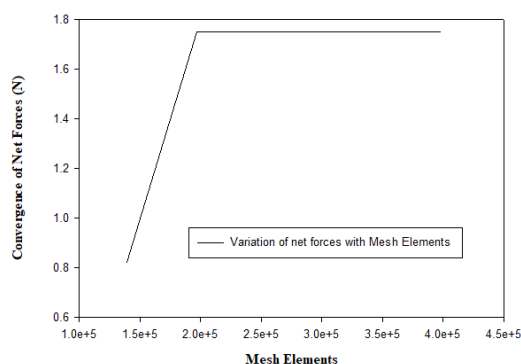


Fig. 8 Mesh independency test for net forces

Table 3 Technical Specifications of Scroll Compressor ZR28KM-PFZ-582

Type of Parameter	Parameter	Value
Mechanical	Displacement	228.6 CFH
	Suction Port	3/4"
	Discharge Port	1/2"
	Oil charge	1 liter
	Net weight	90 Kg
Electrical	Shaft power	2.5 HP
	No. of Phase	1

	Voltage	220-240
	Frequency	50HZ
	LRA	52.9 A
	RLA	13 A
	RPM	2900
Thermodynamic	Refrigerant	R22
	Maximum Pressure Range	27 bar
	Mass Flow Rate	338 lbs/hr
	Electric Power	2020 watts

2.5 Thermodynamic modeling

The built-in volume is the determining factor of the expansion in the scroll expander. The inlet port of a scroll-type expander is located at the center of the stator and rotor, and the scroll wraps are the involute shape of a circle with uniform thickness. The variation of parameters such as mass flow rate, volume, pressure, and temperature of a scroll to an angle of rotation must be determined to carry out a thermodynamic analysis of a scroll-type expander. In the conversion of the scroll compressor to the scroll-type expander, the volumetric ratio must be maintained constant. Temperature, pressure, speed, and mass flow rate are used to calculate the efficiency of a scroll-type expander. The thermodynamic properties are determined using the following relationships.

2.6 Ideal Gas Equation

In this study, the scroll-type expander is powered by compressed air. Assuming no heat transfer, low-pressure compressed air is supplied via the scroll expander's inlet. The working fluid is compressed air and is considered an ideal gas. The thermodynamic properties are investigated using ideal gas equations. GAO. *et.al.* (Wang, 2015) use the ideal gas law to balance the mass equation for scroll-type expanders, ignoring heat transmission and focusing on the internal energy of the equation.

$$\frac{dT}{d\theta} = \frac{1}{m c_v} \left(\frac{dQ}{d\theta} - \frac{dW}{d\theta} + h_{inlet} \frac{dm_{in}}{d\theta} - h_{outlet} \frac{dm_{out}}{d\theta} - u \frac{dm}{d\theta} \right) \quad (4)$$

$$m c_v \frac{dT}{d\theta} = \frac{dQ}{d\theta} - \frac{dW}{d\theta} + h_{inlet} \frac{dm_{in}}{d\theta} - h_{outlet} \frac{dm_{out}}{d\theta} - u \frac{dm}{d\theta} \quad (5)$$

By rearranging the components, the energy balancing equation is reduced to Eq. (5) for determining real work output that deviates from isentropic expansion in the adiabatic condition.

$$\frac{dw}{d\theta} = h_{inlet} \frac{dm_{in}}{d\theta} - h_{outlet} \frac{dm_{out}}{d\theta} \quad (6)$$

According to the scroll-type expander's design, there must be a fixed tolerance in the radial and axial axes for scroll rotation to prevent radial and flank leakage.

$$m_{total} = m_{inlet} + m_{leakage} \quad (7)$$

Eq. 7 can be used to compute the total mass flow rate. The mass flow rate at the inlet and mass leakage in terms of rotating scroll speed is given by

$$m_{total} = \frac{N \cdot V_{swept}}{v_{suc}} + m_{leakage} \quad (8)$$

$$m_{leakage} = \rho A V \quad (9)$$

The leakage area is designated by the letter A. The A_r and A_f are radial and flank leakage lengths, according to Scroll compressor manufacturing design data. Which are calculated using the radial and flank gaps (δ_r and δ_f). The values are listed as 6 microns in the manufacturer's catalog. The nozzle leakage model (Xinjing *et al.*, 2017) is applied to calculate the mass flow rate in chambers in this study.

Depending on the type of expansion, the effect of leakage losses is evaluated. The scroll-type expander exhibits three forms of expansion under-expansion, over-expansion, and optimal expansion. The expansion type is determined by using both isentropic and volumetric efficiency. The following relationships are used to compute volumetric and isentropic efficiency.

$$\eta_{is} = \frac{h_1 - h_2}{h_1 - h_{ideal}} \quad (10)$$

Similarly, isentropic efficiency and mechanical power developed are calculated from the relations

$$\eta_v = \frac{m_{th}}{m_{total}} \quad (11)$$

where η_v is the volumetric efficiency, theoretical mass m_{th} is the mass flow rate in the first chamber without considering leakage loss. By measuring the volume and pressure inside the chamber and using the power generated by the shaft, a scroll expander's mechanical efficiency can be computed Liu G (Liu et al., 2010). The power developed is given as

$$P_w = \eta_m \times \frac{N}{120} \times (\sum(V_{i+1} + V_i) \times (P_{i+1} - P_i)) \quad (12)$$

Scroll efficiency is defined as the ratio of energy obtained from compressed air to the maximum energy supplied by working fluid.

$$\eta_s = \frac{P1V1 + Min(U1 - U2) - P2V2}{Min(h1 - h_{ideal})} \quad (13)$$

3. EXPERIMENTAL EVALUATION

3.1 Setup for the experiment

In a scroll-type expander's geometry, the rotating scroll is placed on top of a stationary scroll. Oldham coupler are used to control the rotating scroll's direction and lessen relative motion between the stationary and rotating scrolls. The scroll-type expander is not properly lubricated. To record the scroll geometry values, the scroll compressor's components are disassembled. Table 1 displays the geometrical features of the measured scroll-type expander. The design includes a flywheel, a rope, and a brake dynamometer is also included. The output port of the scroll compressor has been converted to the input port of the scroll-type expander, and vice versa. The constructed scroll-type expander, as well as the rotating scroll, stationary scroll, and Oldham connection, are depicted in Figure 9.



Fig.9 Stationary & Rotating Scrolls, Oldham coupling, and assembled scroll-type expander

The inlet of the scroll-type expander has been equipped with a pressurized air supply from an air compressor. For flow measurement, rotameters are placed at the entrance and outflow. A pressure gauge and a temperature sensor are employed at the intake and output to measure the pressure and temperature, respectively. Pressure regulators regulate the flow of pressure at the inlet. In the test bench for scroll-type expanders, brake power output is measured using a rope brake dynamometer. The test bench schematic is shown in Figure 10.

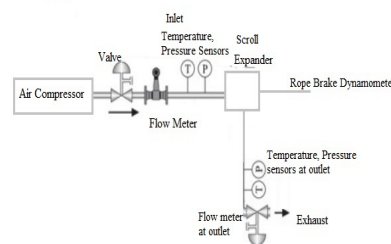


Fig. 10 Schematic of Experimental test bench.

The compressor with a 12 kg air tank and a pressure range of 1 bar to 20.68 bar with a 1 bar pressure cut-off valve supplies compressed air for the scroll-type expander under test. The experimental test bench's schematic is shown in Figure 10. Inlet port, temperature, and pressure are typically measured by a pressure gauge (with an accuracy of ± 0.5 bar) and a temperature sensor (with an accuracy of $\pm 0.01^\circ\text{C}$). The output pressure and temperature are measured with a BMP280 pressure sensor (with an accuracy of $\pm 1\%$), and the flow rate of mass and accumulated volume with time at the inlet and outlet is measured with a flow sensor (with an accuracy of $\pm 0.5\%$). Both devices are programmed in the hardware programming language Arduino and connected to an Arduino board for data acquisition.



Fig. 11 Scroll expander test setup

The various devices connected to the test bench are shown in Figure 11. The manufacturer's catalog is used to calibrate mechanical equipment. Adjusting the sensors involves electrical hardware programming, recording the board's highest and lowest values, and using Arduino programming. A non-contact laser tachometer (with an accuracy of $\pm 0.05\%$) is used to measure the speed in revolutions per minute. A rope and brake dynamometer is used to gauge the mechanical torque and braking power of the scroll-type expander. 0.2 m flywheel and ± 0.01 m rope make up the rope and brake dynamometer. (With a ± 0.05 -gram precision) The dead weights are 500 grams. The research results are compiled in Table 8. The devices for data acquisition utilized to collect experimental test results are shown in Figure 12.



Fig. 12 Flow sensor connected to Arduino board, BMP280 pressure sensor, pressure gauge, and laser tachometer

Under no load conditions, experiments are conducted on the test rig, and the related parameters are presented in Table 4, Table 5, and Table 6.

Table 4 Experimental parameters under no load condition (Trail1)

Inlet Pressure (P ₁) (bar)	Inlet Temperature (T ₁ °C)	Speed (RPM)	Outlet Pressure (P ₂) (bar)	Outlet Temperature (T ₂ °C)
2.06	35.6	1320	0.99	34.9
2.75	35.7	1744	1.011	33.4
3.44	36.2	2600	1.009	33.5
4.13	36.4	3204	1.010	33.6

Table 5 Experimental parameters under no load condition (Trail2)

Inlet Pressure (P ₁) (bar)	Inlet Temperature (T ₁ °C)	Speed (RPM)	Outlet Pressure (P ₂) (bar)	Outlet Temperature (T ₂ °C)
2.06	33.8	1320	0.99	34.9
2.75	34.5	1744	1.011	34.1
3.44	35.8	2600	1.009	34.5
4.13	35.9	3204	1.010	35.1

Table 6 Experimental parameters under no load condition (Trail3)

Inlet Pressure (P ₁) (bar)	Inlet Temperature (T ₁ °C)	Speed (RPM)	Outlet Pressure (P ₂) (bar)	Outlet Temperature (T ₂ °C)
2.06	33.8	1320	0.99	34.9
2.75	34.5	1744	1.011	34.1
3.44	35.8	2600	1.009	34.5
4.13	35.9	3204	1.010	35.1

Three trials were conducted under no load condition until the compressor's input parameters for temperature and pressure remained unchanged. According to CFD simulation, when inlet pressure is set below 1.379 bar, the exit pressure falls below atmospheric, and reverse flow happens. Hence the inlet pressure is set throughout the analysis above 1.379 bar. Further in the experiment, the pressure range has been determined to begin at 2.75 bar for experimentation to get a considerable power output with the load. Similar to this, at pressures of 2.75, 3.44, and 4.13 bar, two trails with mechanical loads ranging from 1 kg to 2.5 kg were conducted to test the accuracy of the results. The experimental test conditions range has been provided in the following Table 7. This study aims to assess performance and determine the maximum and minimum torque produced before critical torque. According to experimental research, a 2.5 kg weight is the critical torque point. Hence the performance evaluation is performed up to 2kg load. Table 8 displays the related values. The work developed and pressure ratio at loaded conditions are stated in Tables 9(a), 9(b), and 9(c).

Table 7 Experimental Test Range

Inlet Pressure (P ₁) (bar)	Inlet Temperature (T ₁ °C)	Speed (RPM)	Outlet Pressure (P ₂) (bar)	Outlet Temperature (T ₂ °C)
2.75	34.5-34.8	1147-1000	1.011-1	34.1-34.5
3.44	35.5-35.8	1350-1100	1.009-1	34-34.5
4.13	35.7-35.8	1900-1100	1.010-1	35-35.6

Table 8 Experimental values of Torque and Power at different load conditions.

Inlet pressure (P ₁) (Bar)	Speed (RPM)	Dead Weight (W) (gms)	Spring weight (S) (gms)	Torque(T) = $(W - s) \times 9.81 \times \frac{(D+d)}{2}$ (N-M)	Power(P) ($2 \times \pi \times N \times T$) / 60 (Watts)
2.75	1147	1000	0.085	1.02	123
2.75	1090	1500	0.092	1.53	175.3
2.75	1083	2000	0.101	2.05	232.5
3.44	1338	1000	0.02	1.03	144
3.44	1307	1500	0.08	1.54	210.3
3.44	1226	2000	0.15	2.044	263
3.44	1136	2500	0.21	3.01	304
4.13	1899	1000	0.05	1.024	204
4.13	1535	1500	0.1	1.53	247
4.13	1506	2000	0.15	2.045	322.4
4.13	1130	2500	0.2	2.55	302.8

Table 9(a) Power and Mechanical efficiency at various load conditions at 2.75 bar pressure.

Inlet pressure (P ₁) (Bar)	Outlet pressure (P ₂) (Bar)	Dead weight (gms)	Pressure ratio	Power (kW)	Mechanical efficiency (%)
2.75	1.011	1000	2.7	0.123	42.07
2.75	1.0115	1500	2.7	0.175	64.4
2.75	1.01146	2000	2.7	0.232	70.05

Table 9(b) Power and Mechanical efficiency at various load conditions at 3.44 bar pressure.

Inlet pressure (P ₁) (Bar)	Outlet pressure (P ₂) (Bar)	Dead weight (gms)	Pressure ratio	Power (kW)	Mechanical efficiency (%)
3.44	1.009	1000	3.4	0.144	28.37
3.44	1.010	1500	3.4	0.210	41.61
3.44	1.011	2000	3.4	0.263	59.57
3.44	1.01	2500	3.4	0.304	72.05

Table 9(c) Power and Mechanical efficiency at various load conditions at 4.13 bar pressure.

Inlet pressure (P ₁) (Bar)	Outlet pressure (P ₂) (Bar)	Dead weight (gms)	PR	Power (kW)	Mechanical efficiency (%)
4.13	1.0103	1000	4.0	0.204	23.93
4.13	1.01033	1500	4.0	0.247	37.01
4.13	1.01	2000	4.0	0.322	53.02
4.13	1.01	2500	4.0	0.302	71.48

4 EXPERIMENTAL DISCUSSIONS AND FINDINGS

The scroll motor test is carried out in the pressure change of 2.75 bar to 4.13 bar with varied mechanical loads and speeds, and the results corresponding to developed power are listed in Table 8. From the thermal relations developed, the performance parameters with load application are evaluated. The expansion process in scroll-type expanders might be one of three sorts. Isentropic expansion, over-expansion, and under-expansion.

If the pressure at the outlet is less than atmospheric, the expansion will be under-expansion, resulting in fluid flow in the opposite direction. To determine the optimal pressure ratio in the low-pressure range, for application development, all performance characteristics are examined against the pressure ratio.

4.1 Power variation in terms of Pressure Ratio and Speed

The input to exit pressure ratio, or pressure ratio, is discovered to be between 2.7 and 4.01. Figure 13 shows a graph illustrating the power variation with pressure ratio. The mechanical power generated with a change in load and pressure ratio is taken into account. Before reaching the critical torque, the power is at its highest with higher loads.

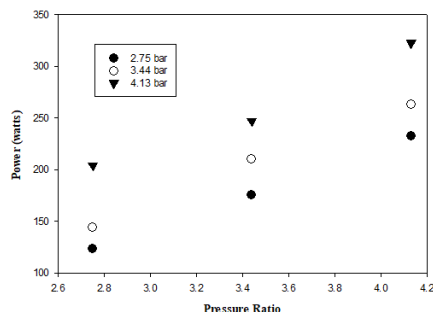


Fig. 13 Experimental Power developed.

Similar to this, Figure 14 displays a curve showing the mechanical power variation with the load. The study has found that increasing the pressure ratio causes more power to be produced for a given load. Additionally, the speed decreased when the weight on the expander shaft increased from 1 kg to 2.5 kg.

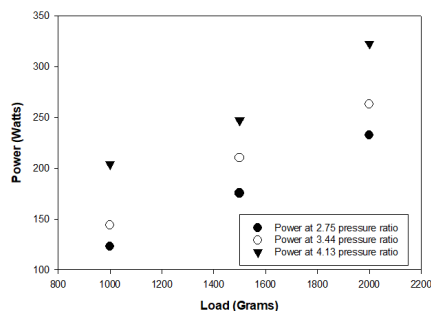


Fig. 14 Variation of Power with Load.

4.2 Experimental Volumetric Efficiency

The outside and inlet of the scroll-type expander were appropriately sealed to achieve higher volumetric efficiency. The density has a direct relationship with the air mass flow rate. Similarly, the square root of the density determines how much air leaks out. As a result, the volumetric efficiency declines as the mass flow rate increases and the air leakage ratio increases. There will be an increase in airflow as the speed rises and the mass flow rate rises. As a result, the volumetric efficiency increases up to a point before declining as the pressure ratio rises due to suction port opening and closing. Analysis of these tests both in CFD and experimental showed that the volumetric efficiency of the scroll-type expander varies not only with speed and pressure difference but also with the change in input temperature. The pressure difference in chambers causes internal leakages in the scroll-type expander. It has been demonstrated that the volumetric efficiency can range from 50% to 83%. The variation of experimental volumetric efficiency obtained has been plotted against the pressure ratio and is given in Figure 15.

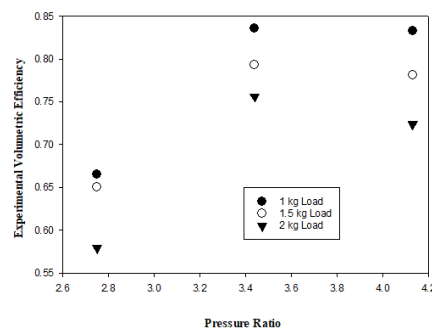


Fig. 15 Variation of volumetric efficiency with pressure ratio

4.3 Experimental Mechanical efficiency as a function of load and pressure ratio

Mechanical efficiency is measured and illustrated in Figure 16 to test the effectiveness of the scroll-type expander with varied loads. In the experimental findings, two notions are investigated. A rise in input pressure causes the speed to increase while the torque decreases under constant load. At constant pressure, on the other hand, when the load increases, the speed decreases, and the torque increases. The mechanical load is regulated between 1kg and 2.5 kg, while the pressure at the inlet is controlled between 2.75 bar and 4.13 bar. The maximum torque is obtained at critical power which is calculated from the rope brake dynamometer. At critical power, mechanical efficiency and torque are reported to be maximum. The graphical representation of the variation of mechanical efficiency with load has been given in Figure 16. Similarly, the mechanical efficiency variation with pressure ratio is presented in Figure 17.

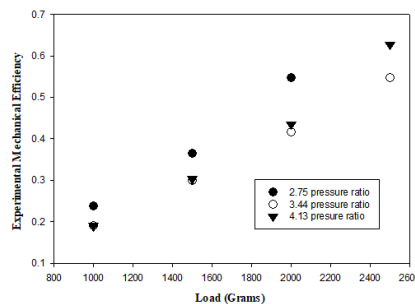


Fig. 16 Variation Mechanical efficiency with the load.

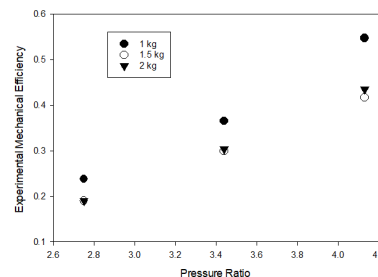


Fig. 17 Variation of Mechanical efficiency with Pressure Ratio.

4.4 Experimental Isentropic efficiency

The experimental isentropic efficiency in the present analysis is found to have similarities with the ideal isentropic expansion given by Moradi Emanuele (MoradiEmanuele et al., 2021). In scroll-type expanders, the pressure ratio is a function of the built-in volume. The built-in volume of

scroll technology is predefined. As a result, scroll-type expanders will have an ideal pressure ratio above which performance characteristics will rise and eventually fall. Figure 18 gives the experimental isentropic efficiency that has been generated with the variation of pressure ratio and at different load conditions.

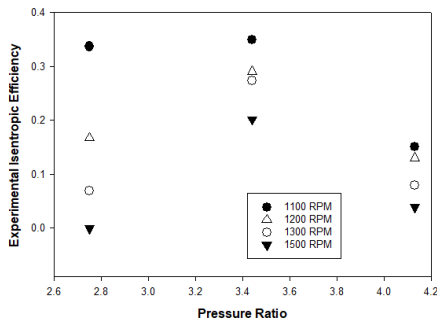


Fig. 18 Experimental isentropic efficiency with pressure ratio.

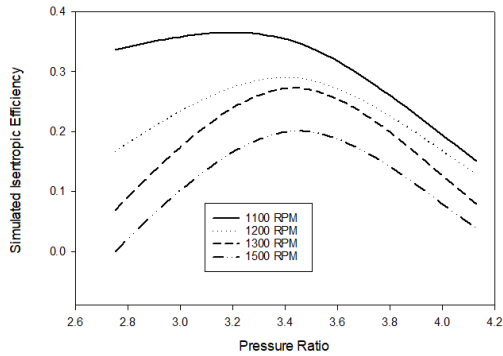


Fig. 19 Simulated Isentropic Efficiency

A similar pattern of increasing to a maximum and then decreasing the isentropic efficiency curve is observed. Simulation and the experimental study revealed a similar trend, with the optimal pressure ratio being in the range of 3-4 for scroll-type expanders and 3.44 for converted scroll-type expanders. Figure 18 gives the experimental isentropic efficiency at various loads and speeds. Figure 19 is the simulated isentropic efficiency variation with pressure ratio. Similarly, Figure 20 gives the isentropic efficiency with pressure obtained by researchers (MoradiEmanuele et al., 2021) for comparison purposes.

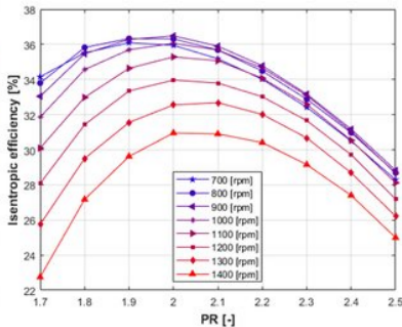


Fig. 20 Ideal Isentropic expansion process in scroll expanders Moradi Emanuele, et al (MoradiEmanuele et al., 2021).

4.5 Experimental Scroll Efficiency

Calculations are made to assess scroll efficiency using the work produced by compressed air, including internal energy. Pressure ratio increases are

accompanied by an increase in scroll expander efficiency. The fluctuation in scroll efficiency with pressure ratio is shown in Figure 21. It has been observed that scroll efficiency has reduced as the load has increased.

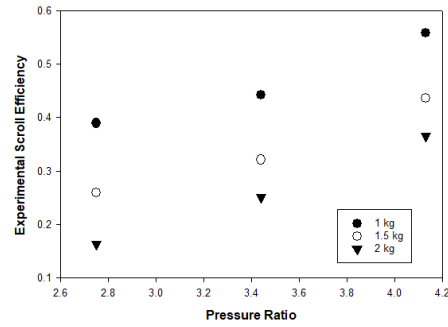


Fig. 21 Scroll efficiency variation with pressure ratio.

4.6 Experiment data versus Simulation model comparison

To validate the research findings, the predicted simulation model with experimental findings is compared to the measured experimental values. The mechanical efficiency is found to increase with the increase in load at various pressures, and a similar pattern has been predicted in simulation. In both simulation and experiment, the highest mechanical efficiency is found to be at 3.44 bar pressure and 2.5 kg of load. Figure 22 gives the comparison between simulated and experimental values for volumetric efficiency.

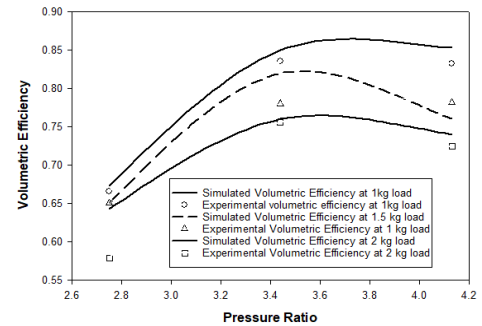


Fig. 22 Effect of pressure ratio on Volumetric efficiency.

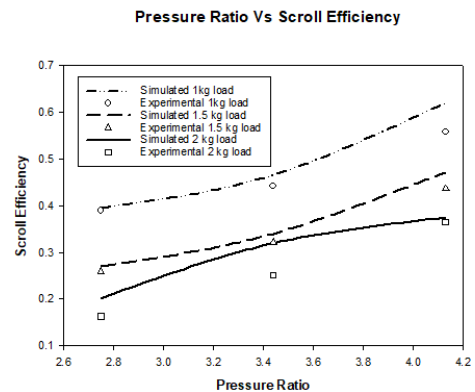


Fig. 23 Effect of pressure ratio on Scroll efficiency

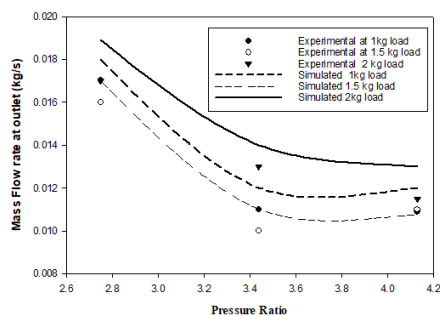


Fig. 24 Effect of Mass Flow rate at the outlet with pressure ratio.

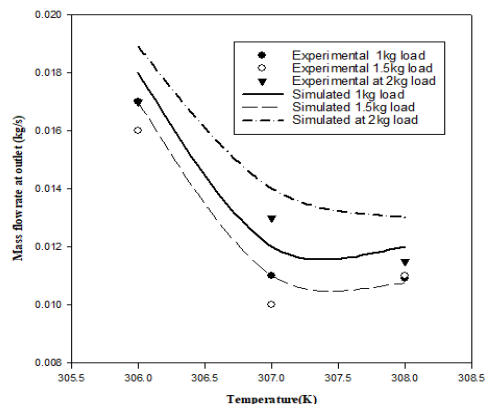


Fig. 25 Effect of Mass flow rate with Temperature.

Figures 22–25 compare the results of simulations and experiments on several performance factors. The discrepancy between the findings of the simulation and experiment is 0.023%.

5 CONCLUSIONS

To generate power with a scroll expander, the determining factors are compressed air supply, inlet pressure, volumetric ratio, and speed. The following conclusions are made from the examination of the experimental results.

- 1) Scroll compressors can work as scroll expanders when operated in reverse.
- 2) Waste heat recovery applications can use scroll expanders, which perform effectively at low pressure.
- 3) As scroll-type expanders are volumetric expanders, the volumetric ratio influences the pressure and mass flow rate at the outlet.
- 4) According to CFD analysis, the under-expansion inside the chambers of scroll-type expanders increases the likelihood of reverse flow at pressures below 1.379 bar.
- 5) Experiment results show that volumetric efficiency decreases with increasing speed, ranging from 83% to 53% at lower speeds and loads.
- 6) The pressure ratio is the determining factor for the isentropic efficiency of a scroll irrespective of the high or low-pressure range. The optimum pressure ratio for scroll expanders is in the range of 3-4.

It can be concluded that when designing a scroll expander for low-pressure range applications, a rise in leakage losses are crucial factors to take into account. The experimental performance characters in the scroll-type expander are in good agreement with the performance characters for simulation in those experimental settings.

Data Availability Statement: The research is in progress, the values obtained in the experiment are within the manuscript and in the supplementary file. The authors have no conflict of interest. The experimental data can be obtained from the corresponding author upon request.

NOMENCLATURE

A	Area
a	Coefficient of force
C_p	Specific heat at constant pressure
C_v	Specific heat at constant volume
F	Net Forces
H	Height
h	Specific Enthalpy ($C_p T$)
i, j	Coordinates in vector notation.
M_A	Net Moments
m	Mass of air in the chamber.
N	Speed
P	Pressure
Q	Heat Transfer rate
R_{AB}	Orbiting Radius
r_{AB}	Moment Vector
R	Universal gas constant
r	Radius
S_m	Source Mass
T	Temperature.
t	Thickness
U	Internal Energy ($mC_v T$)
V	Volume
v	Specific volume
W	Work

Abbreviations

WHR	Waste heat recovery
CFD	Computational fluid dynamics
CFH	Cubic foot per hour.
FVM	Finite volume model
ORC	Organic Rankine Cycle.

Greek Letters

γ	Adiabatic index (C_p/C_v)
δ	Clearance

φ	Involute angle (in degrees)
η	Efficiency
ρ	Density
θ	Angle (degrees)
Suffixes	
b	base
f	Flank
in	Inlet
is	isentropic
m	Mechanical
N	Net Forces
out	Outlet
r	Radial
s	Scroll
suc	Suction
th	Theoretical

REFERENCES

- ANSYS , 2015. *Ansys Theory fluent guide 15*. © SAS IP, Inc.
- ClaudioCampana, 2019. "Experimental analysis of a small-scale scroll expander for low-temperature waste heat recovery in Organic Rankine Cycle". *Energy*, 187
<https://doi.org/10.1016/j.energy.2019.115929>.
- Dieckmann, J., 2017. "Waste Heat-to-Power Using Scroll Expander for Organic Rankine Bottoming Cycle". Technical. US: TIAX LLC, Lexington, MA (United States).
<https://doi.org/10.2172/1360148>
- DOE:US, 2017. "Energy Efficiency and Renewable energy". US.
- Fatigati, 2020. "Experimental characterization of a hermetic scroll expander operating in an ORC-based power unit bottoming a Internal Combustion Engine" 2020. Published by AIP Publishing; ;
<https://doi.org/10.1063/1.5138802>.
- Fatigati, F., Giammarco, Giovine & Cipollone, R., 2022. "Feasibility Assessment of a Dual Intake-Port Scroll Expander Operating in an ORC-Based Power Unit." *Energies*, 15
<https://doi.org/10.3390/en15030770>, p.770.
- Flihahia, E., Sriti, M., Achemlal, D. & haroui, M.E., 2021. "CFD Analysis of free convection in non-darcian porous medium and comparison with similarity approach." *Frontiers in Heat and Mass Transfer* , 17
<https://doi.org/10.5098/hmt.17.7>.
- Gao, Jiang & Wang, 2015. "Simulation and experiments on an ORC system with different scroll expanders based on energy and exergy analysis". *Applied Thermal Engineering*,
<https://doi.org/10.1016/j.applthermaleng.2014.10.044>.
- Hijriawan, M. et al., 2022. "Experimental analysis of R134a working fluid on Organic Rankine Cycle (ORC) systems with scroll-expander." *Engineering Science and Technology, an International Journal*, 29
<https://doi.org/10.1016/j.jestech.2021.06.016>.
- LaftaSarmad, F., FakhruddinMuhammad, K. & EleiwiMuhammad, A., 2022. "Cfd simulation in thermal-hydraulic analysis of air flow on different attack angles of row flat tube." *Frontiers in Heat and Mass Transfer* , 19
<https://doi.org/10.5098/hmt.19.6>
- Lee & Wu, 1996. "A study of planar orbiting mechanism and its applications to scroll fluid machinery." *mechanism and machine theory*, 31
[https://doi.org/10.1016/0094-114X\(95\)00116-G](https://doi.org/10.1016/0094-114X(95)00116-G).
- Liu, Zhao, Lil & Shu, 2010. "Simulation and experiment research on wide ranging working process of scroll expander driven by compressed air." *Applied Thermal Engineering*, 30
<https://doi.org/10.1016/j.applthermaleng.2010.05.015>.
- Lu, Y., 2015. "Experimental investigation of a scroll expander for power generation part of a resorption cogeneration." In *The 7th International Conference on Applied Energy – ICAE2015*., 2015.
<https://doi.org/10.1016/j.egypro.2015.07.356>.
- MoradiEmanuele, R. et al., 2021." Component-Oriented Modeling of a Micro-Scale Organic Rankine Cycle System for Waste Heat Recovery Applications." *Applied Sciences* , 11
<https://doi.org/10.3390/app11051984>.
- Moro & Pinamonti, 2008. "ORC Technology systems-wood energy conversion in furniture manufacturing industry." *Thermal science*, 4(12);
<https://doi.org/10.2298/TSCI0804061M>.
- Narasimhan, A.K., 2019. "Mapping scroll expander performance for organic working fluids using dimensionless parameters in Ns-Ds diagram." *Science Direct*,
<https://doi.org/10.1016/j.energy.2019.06.054>.
- Panigrahi, S.S., Singh, C.B. & John, F., 2020." CFD modelling of physical velocity and anisotropic resistance components in a peaked stored grain with aeration ducting systems." *Computers and Electronics in Agriculture*,
doi.org/10.1016/j.compag.2020.105820.
- Qiu, Thomad & Douglas, 2018. "Investigation of a scroll expander driven by compressed air and its potential applications to the ORC." *Applied Thermal Engineering*, 135
<https://doi.org/10.1016/j.applthermaleng.2018.01.118>.
- RaminMoradi, MauroVillarini & LucaCioccolantici, 2021. "Experimental modeling of a lubricated, open drive scroll expander for micro-scale organic Rankine cycle systems." *Applied Thermal Engineering*, 190
<https://doi.org/10.1016/j.applthermaleng.2021.116784>.
- Simon Emhardt, 2018. "A review of scroll expander geometries and their performance." *Applied Thermal Engineering*,
<https://doi.org/10.1016/J.APPLTHERMALENG.2018.06.045>.
- Tomasz, Z.Kaczmarczyk, Grzegorz & ywica, 2022. "Experimental research of a micropower volumetric expander for domestic applications at constant electrical load." *Sustainable Energy Technologies and Assessments*,
<https://doi.org/10.1016/j.seta.2021.101755>.

Troli, P.-s., 2019. "CFD simulations in a blade cascade rig." *Energy and Environmental Engineering*.

Wei, J. et al., 2022. "A review of the research status of scroll expander." *Institute of Mechanical Engineers*,
<https://doi.org/10.1177/09576509221109245>.

Xinjing, Xu, Jian & Yong, 2017. "Study on performance and optimization of a scroll expander driven by compressed air." *Applied Energy*, 186

<https://doi.org/10.1016/j.apenergy.2016.06.004>.

YijiLu, 2017. "Conceptual study of scroll-type rotary gasoline Internal Combustion Engine." *Energy Procedia*,
<https://doi.org/10.1016/j.egypro.2017.12.606>.

Zhiwei, Bao & Roskilly, 2016. "Dynamic modeling and experimental validation of scroll expander for small scale power generation system." *Applied Thermal Engineering*,
<https://doi.org/10.1016/j.apenergy.2016.08.025>.